Transient Effects on Microchannel Electrokinetic Filtering with an Ion-Permselective Membrane

Rahul Dhopeshwarkar,[†] Richard M. Crooks,*,[‡] Dzmitry Hlushkou,[§] and Ulrich Tallarek*,[‖]

Department of Chemical Engineering, Texas A&M University, 3122 TAMU, College Station, Texas 77843-3122, Department of Chemistry and Biochemistry, The University of Texas at Austin, 1 University Station, A5300, Austin, Texas 78712-0165, Institut für Verfahrenstechnik, Otto-von-Guericke-Universität Magdeburg, Universitätsplatz 2, 39106 Magdeburg, Germany, and Department of Chemistry, Philipps-Universität Marburg, Hans-Meerwein-Strasse, 35032 Marburg, Germany

The electrokinetics and hydrodynamics in a hybrid microfluidic/nanofluidic pore network configuration and its effect on the concentration enrichment of charged analytes are described. A hydrogel microplug, photopolymerized in a microfluidic channel, with negative surface charge serves as a nanoporous membrane and dictates the electrokinetic behavior within the adjoining microchannel compartments. The nanoporous hydrogel with a mean pore size on the order of the electrical double layer thickness imparts ion-permselectivity (cation-selectivity) to the migration of ionic species which, under the influence of an applied electrical field, drives concentration polarization in bulk solution near the interfaces between the two microchannel compartments and the hydrogel-based nanopores. The concentration enrichment efficiency for charged analytes depends on this concentration polarization, which strongly affects the distribution of local electrical field strength. In addition, electroosmotic flow in the device plays a critical role in determining the location of the analyte enrichment zone. A theoretical model and simulations are presented to explain the interplay of concentration polarization and electroosmotic flow with respect to the observed concentration enrichment of negatively charged analytes at the cathodic hydrogel plug–microchannel solution interface.

The establishment of microscale analysis systems is complemented by current efforts directed to a further decrease of channel sizes toward nanometer dimensions.[1,2] This development can become an important step in the lab-on-a-chip concept, which is well-suited to small-scale analysis combined with high throughput. Nanoscale fluidic channels also provide access to a new regime in the fundamental study of fluid and molecular transport in confined geometries. Of particular interest is the influence of the surface charge density, nanopore size and shape, mobile phase ionic strength, and mass-to-charge ratio of ionic species in the electrolyte solution on the inherently coupled mass and charge transport through discrete nanochannels or devised nanochannel networks.[3–10]

While the typical thickness of the electrical double layer (EDL) remains much smaller than micrometer-sized fluidic channels, it often approaches typical nanopore sizes. Thus, compared to microfluidic channels which are usually used for transporting bulk liquid and analytes by electroosmotic flow (EOF), nanopores can be employed to control the transferred ionic current depending on their ion-permselectivity. The ion-permselectivity of single nanopores, as well as its consequences for molecular and ionic transport are also reflected in the corresponding macroscopic behavior of nanoporous membranes which are essentially networks of nanopores. In particular, the control of pore size, pH, and ionic strength of the external mobile phase, as well as surface charge allows one to direct transmembrane mass and charge transport through a multiple-barrier approach.[11–17] An important implication of the ionic conductance of ion-permselective membranes is that under the influence of an applied electrical field, concentration polarization (CP) develops. CP is a complex effect related to the formation of concentration gradients of ionic species in the bulk electrolyte solution adjacent to a charge-selective interface upon the passage of electrical current normal to that interface.[18]

* Authors to whom correspondence should be addressed. E-mail: crooks@cm.utexas.edu (R.M.C.); tallarek@staff.uni-marburg.de (U.T.).
† Texas A&M University.
‡ University of Texas at Austin.
§ Otto-von-Guericke-Universität Magdeburg.
‖ Philipps-Universität Marburg.

(1) Mijatovic, D.; Eijkel, J. C. T.; van den Berg, A. *Lab Chip* **2005,** *5,* 492–500.
(2) Perry, J. L.; Kandlikar, S. G. *Microfluid. Nanofluid.* **2006,** *2,* 185–193.
(3) Woermann, D. *Phys. Chem. Chem. Phys.* **2004,** *6,* 3130–3132.
(4) Karnik, R.; Fan, R.; Yue, M.; Li, D.; Yang, P.; Majumdar, A. *Nano Lett.* **2005,** *5,* 943–948.
(5) Siwy, Z.; Kosinska, I. D.; Fulinski, A.; Martin, C. R. *Phys. Rev. Lett.* **2005,** *94,* 048102.
(6) Schoch, R. M.; van Lintel, H.; Renaud, P. *Phys. Fluids* **2005,** *17,* 100604.
(7) Ho, C.; Qiao, R.; Heng, J. B.; Chatterjee, A.; Timp, R. J.; Aluru, N. R.; Timp, G. *Proc. Natl. Acad. Sci. U.S.A.* **2005,** *102,* 10445–10450.
(8) Smeets, R. M. M.; Keyser, U. F.; Krapf, D.; Wu, M.-Y.; Dekker, N. H.; Dekker, C. *Nano Lett.* **2006,** *6,* 89–95.
(9) Siwy, Z. S. *Adv. Funct. Mater.* **2006,** *16,* 735–746.
(10) Cervera, J.; Schiedt, B.; Neumann, R.; Mafé, S.; Ramirez, P. *J. Chem. Phys.* **2006,** *124,* 104706.
(11) Nishizawa, M.; Menon, V. P.; Martin, C. R. *Science* **1995,** *268,* 700–702.
(12) Martin, C. R.; Nishizawa, M.; Jirage, K.; Kang, M. *J. Phys. Chem. B* **2001,** *105,* 1925–1934.
(13) Chun, K.-Y.; Stroeve, P. *Langmuir* **2002,** *18,* 4653–4658.
(14) Ku, J.-R.; Stroeve, P. *Langmuir* **2004,** *20,* 2030–2032.
(15) Ramirez, P.; Mafé, S.; Alcaraz, A.; Cervera, J. *J. Phys. Chem. B* **2003,** *107,* 13178–13187.
(16) Lee, S. B.; Martin, C. R. *Anal. Chem.* **2001,** *73,* 768–775.
(17) Chun, K.-Y.; Mafé, S.; Ramirez, P.; Stroeve, P. *Chem. Phys. Lett.* **2006,** *418,* 561–564.

The need for a detailed analysis of ionic currents through ion-permselective interfaces has recently been recalled through a variety of functional devices which have been constructed by integrating discrete nanochannels or nanoporous materials in microscale analysis systems to form hierarchically structured hybrid microfluidic/nanofluidic architectures for, e.g., improved sample preparation, separation, and detection.[19-37] These devices demonstrate specific morphologies and interconnectivities between microfluidic and nanofluidic elements, depending on the application. In particular, powerful sample preconcentration strategies have been demonstrated. This trend is further stimulated by the straightforward in situ preparation and integration of membrane units and the easy control of the applied electrical fields. On the other hand, the whole electrokinetic and hydrodynamic complexity associated with CP is usually also "integrated" into such devices and must be carefully addressed for tailoring desired ionic transport but minimizing adverse effects.

In this paper we analyze the interplay of transient effects within a microfluidic channel that incorporates a negatively charged hydrogel plug. The electrokinetic behavior of this system and device performance can be described in terms of the development and interplay of CP and EOF. The hydrogel microplug, having fixed negative charges on its backbone and a mean pore size on the order of the EDL thickness, behaves as a cation-permselective membrane (Figure 1). Under the influence of an applied electrical field, the imbalance between ionic fluxes within the hydrogel and the microchannel results in the enrichment of negatively charged tracer molecules near the interface between the cation-selective hydrogel and the bulk solution in the cathodic compartment of the microfluidic device (inset of Figure 1). The intensity and interplay of CP and EOF, which both originate from the negative surface charge on the nanoporous hydrogel plug, determine the
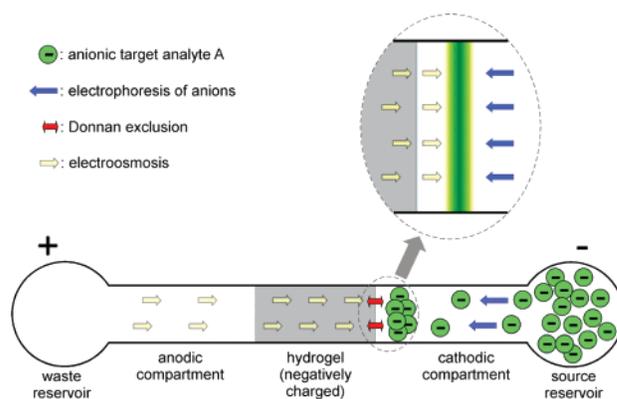

Figure 1. Schematic illustration of transport processes in the microfluidic device containing an immobilzed, negatively charged hydrogel microplug with a mean pore size comparable to the electrical double layer thickness.

magnitude of this enrichment and its location, thus, the overall concentration enrichment efficiency of the device.

The experimental approach presented here complements previous related reports from our group.[22,28] For example, we showed that a three-dimensional microfluidic system, consisting of a thin nanoporous polyester membrane sandwiched between two microfluidic channels, could be used to concentrate DNA.[22] However, this type of device was difficult to reproducibly fabricate, and therefore we adopted an analogous two-dimensional system for subsequent studies. The two-dimensional device consisted of a single microfluidic channel divided into two compartments by a photopolymerized hydrogel microplug.[28,38] In this configuration, the nanopores within the hydrogel act as fluidic transport modulators. This design is much easier to fabricate than the three-dimensional system and results in concentration enrichment of negatively charged analytes such as single-stranded DNA (ssDNA) and fluorescein. For example, it was possible to achieve a ~500-fold enrichment of ssDNA in just 150 s using potentials on the order of ~100 V. In the present study we have further simplified the microfluidic system to ease efforts to fully understand the electrokinetic principles governing its behavior. We provide a theoretical model and computer simulations that are qualitatively consistent with experimental observations of analyte enrichment in the vicinity of negatively charged 2-hydroxyethyl methacrylate (HEMA) hydrogel microplugs contained within poly(dimethylsiloxane) (PDMS)/glass microfluidic channels.

EXPERIMENTAL SECTION

Chemicals. Precursors for preparing PDMS (Sylgard 184) microfluidic devices were obtained from K. R. Anderson, Inc. (Morgan Hill, CA). Fluorescein disodium salt (98+%, Avocado, Heysham, England), and 5′-carboxyfluorescein-labeled 22-mer ssDNA (IDT, Coralville, IA) were used as analytes. Acrylic acid, HEMA, ethylene glycol dimethacrylate, and Irgacure 651 (Sigma-Aldrich, St. Louis, MO) were used as received. The 10.0 mM TRIS−HCl buffer (pH 8.1) used in all experiments was prepared by diluting molecular biology grade 1 M TRIS−HCl buffer (Fisher Biotech, Fair Lawn, NJ) with deionized water (18 MΩ cm, Milli-Q gradient system, Millipore).

(18) Levich, V. G. *Physicochemical Hydrodynamics*; Prentice Hall: Englewood Cliffs, NJ, 1962.

(19) Slentz, B. E.; Penner, N. A.; Regnier, F. E. *J. Chromatogr., A* **2002**, *948*, 225−233.

(20) Hollman, A. M.; Bhattacharyya, D. *Langmuir* **2002**, *18*, 5946−5952.

(21) Cao, H.; Tegenfeldt, J. O.; Austin, R. H.; Chou, S. Y. *Appl. Phys. Lett.* **2002**, *81*, 3058−3060.

(22) Dai, J.; Ito, T.; Sun, L.; Crooks, R. M. *J. Am. Chem. Soc.* **2003**, *125*, 13026−13027.

(23) Kuo, T.-C.; Cannon, D. M., Jr.; Chen, Y.; Tulock, J. J.; Shannon, M. A.; Sweedler, J. V.; Bohn, P. W. *Anal. Chem.* **2003**, *75*, 1861−1867.

(24) Leinweber, F. C.; Tallarek, U. *Langmuir* **2004**, *20*, 11637−11648.

(25) Song, S.; Singh, A. K.; Kirby, B. J. *Anal. Chem.* **2004**, *76*, 4589−4592.

(26) Zapf, R.; Hessel, V. *Chem.-Ing.-Tech.* **2004**, *76*, 513−514.

(27) Kuo, T.-C.; Kim, H.-K.; Cannon, D. M., Jr.; Shannon, M. A.; Sweedler, J. V.; Bohn, P. W. *Angew. Chem., Int. Ed.* **2004**, *43*, 1862−1865.

(28) Dhopeshwarkar, R.; Sun, L.; Crooks, R. M. *Lab Chip* **2005**, *5*, 1148−1154.

(29) Leinweber, F. C.; Pfafferodt, M.; Seidel-Morgenstern, A.; Tallarek, U. *Anal. Chem.* **2005**, *77*, 5839−5850.

(30) Foote, R. S.; Khandurina, J.; Jacobson, S. C.; Ramsey, J. M. *Anal. Chem.* **2005**, *77*, 57−63.

(31) Wang, Y.-C.; Stevens, A. L.; Han, J. *Anal. Chem.* **2005**, *77*, 4293−4299.

(32) Schmuhl, R.; Nijdam, W.; Sekulić, J.; Roy Chowdhury, S.; van Rijn, C. J. M.; van den Berg, A.; ten Elshof, J. E.; Blank, D. H. A. *Anal. Chem.* **2005**, *77*, 178−184.

(33) Plecis, A.; Schoch, R. B.; Renaud, P. *Nano Lett.* **2005**, *5*, 1147−1155.

(34) Hatch, A. V.; Herr, A. E.; Throckmorton, D. J.; Brennan, J. S.; Singh, A. K. *Anal. Chem.* **2006**, *78*, 4976−4984.

(35) Kim, S. M.; Burns, M. A.; Hasselbrink, E. F. *Anal. Chem.* **2006**, *78*, 4779−4785.

(36) Höltzel, A.; Tallarek, U. *J. Sep. Sci.* **2007**, *30*, 1398−1419.

(37) Kim, S. J.; Wang, Y.-C.; Lee, J. H.; Jang, H.; Han, J. *Phys. Rev. Lett.* **2007**, *99*, 044501.

(38) Beebe, D. J.; Moore, J. S.; Bauer, J. M.; Yu, Q.; Liu, R. H.; Devadoss, C.; Jo, B.-H. *Nature* **2000**, *404*, 588−590.
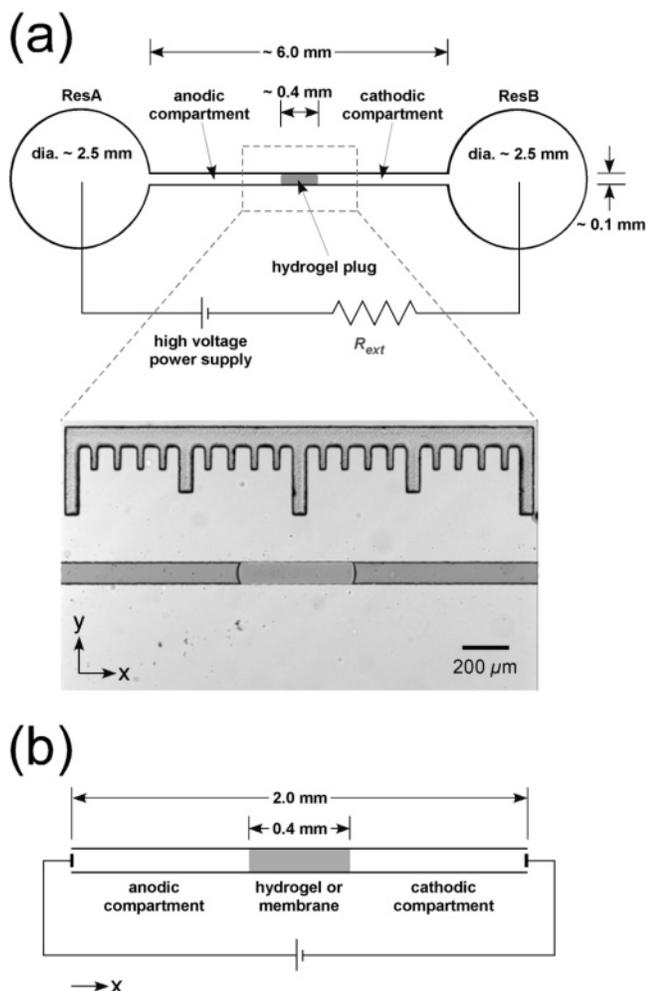
(a)

(b)

Figure 2. (a) Schematic illustration of the microfluidic device used for the electrokinetic concentration enrichment studies. The enlarged view is a microscopic optical image (4× objective lens) of a channel section incorporating a hydrogel microplug. A 2 mm internal scale bar was also embedded in the microfluidic design as a reference for hydrogel polymerization. The enlarged view demonstrates how the region of interest was defined for obtaining the fluorescence intensity profiles along the channel. (b) Schematic illustration of the system used to simulate analyte concentration enrichment in a microfluidic device containing an ion-permselective membrane.

Microfluidic Device Fabrication. The fabrication of PDMS/glass hybrid microfluidic devices employed for the concentration enrichment experiments followed a replica molding procedure described in the literature.[39] First, reservoirs for fluidic delivery were created by punching holes (∼2.5 mm diameter) into a PDMS monolith (∼5 mm thick) containing the microchannel system. The monolith was then washed with ethanol and dried under a stream of N_2 gas. It was then bonded irreversibly to a precleaned cover glass (25 mm × 25 mm, 0.13−0.17 mm thick, VWR Scientific) after both were treated with an O_2 plasma (60 W, model PDC-32G, Harrick Scientific, Ossining, NY) for 15 s. Bonding was carried out for at least 2 min before introducing liquids into the microchannel. The resulting microfluidic architecture (Figure 2a) included a straight microchannel (approximately 100 μm wide, 20 μm deep, and 6 mm long) terminating in the two reservoirs

(39) McDonald, J. C.; Duffy, D. C.; Anderson, J. R.; Chiu, D. T.; Hongkai, W.; Schueller, O. J. A.; Whitesides, G. M. *Electrophoresis* **2000**, *21*, 27−40.

(ResA and ResB). In contrast to the microfluidic device used in our previous studies,[28] this design does not incorporate the side-channels used to remove the unwanted hydrogel precursor from the channel following photopolymerization. This new design, which greatly simplifies modeling, was enabled by the development of an electrokinetic strategy for removing unpolymerized hydrogel precursor (vide infra).

Hydrogel Microplug Fabrication. The hydrogel microplug was incorporated into the microchannel by photopolymerization of an appropriate hydrogel precuror. First, the precursor solution was introduced into the microchannel by capillary action. Next, UV light (365 nm, 200 s, 300 mW/cm², EFOS Lite E3000, Ontario, Canada) was projected onto the central part (∼400 μm long) of the channel from the side port of a microscope (DIAPHOT 300, Nikon) through a 10× objective lens. This resulted in polymerization of the precursors in the illuminated region. To remove the unpolymerized precursor solution, reservoirs ResA and ResB were filled with 10.0 mM TRIS−HCl buffer (pH 8.1), and this buffer solution was allowed to diffuse into the microchannel for about 90 min. Next, voltages ranging from 50 to 150 V were applied between two coil electrodes (90% Pt/10% Ir, 0.25 mm diameter and 50.0 mm in length) immersed in the two reservoirs. The necessary electrical bias was applied using a custom-built, high-voltage (range 0−1067 V) power supply unit using a single output module of a high-power, C-series voltage source (Ultra Volt, Ronkonkoma, NY). Applied voltages could be changed with 100 ms time resolution using custom software. The conditioning step removes unwanted precursor, which bears a negative charge, from the vicinity of the polymerized hydrogel via electrophoresis.

Data Acquisition and Analysis. After conditioning, ResA and ResB were rinsed with 10.0 mM TRIS−HCl buffer, and then 25 μL of 5.0 μM fluorescent analyte (fluorescein or fluorescein-labeled 22-mer ssDNA) in 10.0 mM TRIS−HCl buffer was introduced into each reservoir. A bias voltage was established between the electrodes in the two reservoirs, and simultaneously a set of fluorescence micrographs was captured (V++ microscopy imaging, Digital Optics, New Zealand) from the channel region near the hydrogel using an inverted epifluorescence microscope (Eclipse TE 2000-U, Nikon, Japan) equipped with a CCD camera (Cascade 512B, Photometrics, Tuscon, AZ). A typical capture sequence included 541 frames (4× objective lens, 1 × 1 binning, 512 × 290 pixels) at a rate of 2 s/frame (exposure time 100 ms) spanning a time period of 1080 s. For enhanced visual quality, the images were modified to an appropriate grayscale and a false color scheme was applied (brightness decreasing in the order white-green-blue-black). During application of the electrical bias, the voltage drop across an external resistor R_{ext} (510 kΩ) connected in series with the microfluidic channel (Figure 2a) was recorded using a multimeter.

To analyze the fluorescence intensities and corresponding enrichment factors in the microfluidic system, the entire channel section under the microscopic view was chosen as a region of interest (ROI, inset of Figure 2a). The width-averaged (averaged along the *y*-axis) fluorescence intensity profiles were obtained along the channel (*x*-axis) over the entire ROI at different time intervals. The corresponding enrichment factors were calculated by dividing the peak heights in the fluorescence intensity profiles by the average fluorescence intensity obtained in a reference

channel containing just the original fluorescent analyte. All fluorescence intensity values were corrected by subtracting the background count and normalized before plotting fluorescence intensity profiles.

THEORETICAL BACKGROUND AND MATHEMATICAL DESCRIPTION

Because of the great scientific and technological importance of electrokinetic transport in systems containing ion-exchange membranes, a large number of studies has been devoted to its theoretical description and understanding. However, the complete theory faces some very difficult problems, so that even at the present time certain fundamental issues have not been satisfactorily resolved. Most theoretical studies use a description based on the generalized Maxwell−Stefan (GMS) theory of irreversible thermodynamics. This approach represents a simple mathematical tool to inter-relate the flux of a species through a membrane with the interfacial concentrations of this species at both membrane−solution interfaces, as well as with external driving forces. However, irreversible thermodynamics treats the membrane as a "black box" and does not consider its geometry and topology, microscopic physicochemical parameters, and their relation to macroscopic characteristics. In contrast, another approach based on structure−kinetic models[40−42] takes into account the structural heterogeneity of the membrane and thus makes it possible to establish interrelations between the microscopic characteristics of a membrane and its macroscopic transport behavior (electro-conductivity and diffusion permeability) through so-called transport−structural parameters, which include two structural and two transport parameters.[42] The drawbacks of the latter approach are its inability to provide a spatiotemporal picture of the ion concentrations and local electrical field and its inability to address possible convective transport in a system.

Most descriptions of ionic transport in membranes simplify the GMS description to the Nernst−Planck equation with only two contributions in the ionic transport: diffusion and electromigration. Combining the Nernst−Planck equation with a proper description of the momentum transfer by the Navier−Stokes equation and the electrostatics by the Poisson equation suffices to completely specify the mass transport of ions. The absence of convective transport is frequently invoked as a simplification, which makes it possible to eliminate the Navier−Stokes equation from the mathematical description. Nevertheless, solving the time-dependent coupled Nernst−Planck and Poisson equations leads to considerable difficulties, because at this point no general analytical solution has been obtained. Therefore, numerical methods are commonly employed to solve appropriate balances of components and equations for distributions of the local electrical potential in systems with a charge-selective membrane.[43−48] The numerical simulation of

electrokinetic transport in such systems is still a nontrivial problem, especially if two-dimensional and three-dimensional spatiotemporal patterns have to be resolved.

In this study we employed an approach based on the numerical solution of the coupled Nernst−Planck and Poisson equations as well as the continuity equations in order to simulate electrokinetic transport in the microfluidic system illustrated by Figure 2a. The geometry of the simulated device shown in Figure 2b is reduced to a straight microchannel ($L = 2$ mm) fitted with a flat, porous membrane (400 μm in length) at its center; that is, the membrane covers the distance from $x = 800$ μm to $x = 1200$ μm. It is assumed that the microchannel is terminated in two relatively large reservoirs containing electrodes. The membrane is considered as a pseudo-homogeneous material, i.e., as a homogeneous domain characterized by effective morphological, material, and transport characteristics (dielectric constant, volume density of the fixed electrical charge, etc). In addition, it is assumed that the system is isothermal, in particular, there are no Joule heating effects and that there is no chemical reaction in the system (including water dissociation) and adsorption−desorption taking place at the solid−liquid (wall and membrane) interfaces. Finally, it is assumed that no wall-effects exist and, therefore, the geometry can be reduced to a one-dimensional configuration where all parameters vary only along the x-axis (cf. Figure 2b).

The general transport of ions of the buffer solution and of the analyte molecules due to an applied bias is governed by a conservation law

$$\frac{\partial c_i(x, t)}{\partial t} = \frac{\partial}{\partial x}\left(D_i(x)\frac{\partial c_i(x, t)}{\partial x} + z_i c_i(x, t)D_i(x)\frac{F}{RT}\frac{\partial \phi(x, t)}{\partial x}\right) \quad (1)$$

where c_i is the molar concentration of ionic species i, D_i and z_i are its diffusion coefficient and valency, respectively, ϕ is the local electrical potential, and F, R, and T represent the Faraday constant, molar gas constant, and temperature, respectively.

The local concentration of the ions and the local electrical potential are related by the Poisson equation

$$\frac{\partial^2\phi(x, t)}{\partial x^2} = -\frac{\rho_{\text{fix}}}{\epsilon_0\epsilon_{\text{r}}} - \frac{\rho_{\text{e}}(x, t)}{\epsilon_0\epsilon_{\text{r}}} = -\frac{\rho_{\text{fix}}}{\epsilon_0\epsilon_{\text{r}}} - \frac{F}{\epsilon_0\epsilon_{\text{r}}}\sum_i z_i c_i(x, t) \quad (2)$$

where ρ_{e} is the volume charge density of the electrolyte solution, ρ_{fix} is the volume fixed-charge density of the membrane associated with the surface charge on the pore walls, and ϵ_0 and ϵ_{r} are the vacuum permittivity and dielectric constant, respectively. The value of ρ_{fix} is determined by the surface charge density on the membrane pore walls and by the volume-to-surface ratio for the membrane. As mentioned above, in general, the coupled eqs 1 and 2 have to be complemented by the generalized Navier−Stokes equation (with the electrical term)

(40) Zabolotsky, V. I.; Nikonenko, V. V. *J. Membr. Sci.* **1993**, *79*, 181−198.

(41) Nikonenko, V.; Zabolotsky, V.; Larchet, C.; Auclair, B.; Pourcelly, G. *Desalination* **2002**, *147*, 369−374.

(42) Gnusin, N. P.; Berezina, N. P.; Kononenko, N. A.; Dyomina, O. A. *J. Membr. Sci.* **2004**, *243*, 301−310.

(43) Manzanares, J. A.; Murphy, W. D.; Mafé, S.; Reiss, H. *J. Phys. Chem.* **1993**, *97*, 8524−8530.

(44) Šnita, D.; Pačes, M.; Lindner, J.; Kosek, J.; Marek, M. *Faraday Discuss.* **2001**, *120*, 53−66.

(45) Zabolotskii, V. I.; Manzanares, J. A.; Mafé, S.; Nikonenko, V. V.; Lebedev, K. A. *Russ. J. Electrochem.* **2002**, *38*, 819−827.

(46) Nikonenko, V.; Lebedev, K.; Manzanares, J. A.; Pourcelly, G. *Electrochim. Acta* **2003**, *48*, 3639−3650.

(47) Volgin, V. M.; Davydov, A. D. *J. Membr. Sci.* **2005**, *259*, 110−121.

(48) Quenneville, E.; Buschmann, M. D. *J. Membr. Sci.* **2005**, *265*, 60−73.

$$\rho_f \left(\frac{\partial u(x, t)}{\partial t} + u(x, t) \frac{\partial u(x, t)}{\partial x} \right) = -\frac{\partial p(x, t)}{\partial x} + \mu \frac{\partial^2 u(x, t)}{\partial x^2} - \rho_e(x, t) \frac{\partial \phi(x, t)}{\partial x} \quad (3)$$

where ρ_f and μ are the mass density and dynamic viscosity of the fluid, respectively, and p is hydrostatic pressure. In addition, the Nernst–Planck equation (eq 1) is extended by a term corresponding to the convective component of species fluxes

$$\frac{\partial c_i(x, t)}{\partial t} = \frac{\partial}{\partial x} \left(D_i(x) \frac{\partial c_i(x, t)}{\partial x} + z_i c_i(x, t) D_i(x) \frac{F}{RT} \frac{\partial \phi(x, t)}{\partial x} - c_i(x, t) u(x, t) \right) \quad (4)$$

where u is the local flow velocity. If any flow in the system is absent, i.e., $u(x,t) = 0$, eq 4 is reduced to eq 1. Otherwise (if $u \neq 0$), the convective transport affects the spatiotemporal distribution of the species and needs to be accounted for explicitly.

Generally, the flow velocity field must be determined by resolving the coupled partial differential eqs 2–4. To avoid this mathematically formidable problem in the present study, we employed the following simplified approach. Because of the incompressibility of the fluid its velocity in the anodic and cathodic compartments of the microchannels ($u_{an,cath}$) is related to the average velocity through the hydrogel plug (u_{plug}) as

$$u_{an,cath} = \epsilon u_{plug} \quad (5)$$

where ϵ is the porosity of the hydrogel plug. The volumetric flow and volume-averaged velocity in the whole system are constant. Then, convective transport through the microplug considered as a pseudo-homogeneous medium can be described in terms of an effective velocity $u_{plug}^* = \epsilon u_{plug}$ and eq 5 is reduced to

$$u_{an,cath} = u_{plug}^* \quad (6)$$

The resistance of the microplug to hydraulic flow is very high because of the nanometer-sized pores. Therefore, one can neglect hydraulic flow by pressure gradients induced at the plug–solution interfaces due to changes in the cross-sectional area available for fluid flow and the mismatch of ζ-potentials associated with the generally different (microchannel and hydrogel) surfaces. Hence, to a first approximation the EOF velocity can be introduced into the model as a constant and independent parameter.

In this paper, we use the EOF velocity u calculated by the Helmholtz–Smoluchowski equation, corrected by an arbitrary factor f

$$u = -\frac{\epsilon_0 \epsilon_r \zeta V}{L \mu} f \quad (7)$$

where V is the applied bias. The Helmholtz–Smoluchowski equation makes it possible to determine the EOF velocity in an open homogeneous channel in the thin-EDL-limit. The correction factor f accounts for the effects of the gel porosity, the mismatch

of ζ-potentials for the surfaces of the microchannel and the gel matrix, as well as the EDL interaction (or overlap) within the nanometer-sized pores of the hydrogel. In general, the precise value of this factor is difficult to calculate or determine experimentally. In this study we use $f = 0.1$.

Thus, the spatiotemporal behavior of the ionic concentrations can be obtained by solution of the coupled partial differential eqs 2 and 4 subjected to the corresponding boundary and initial conditions, and eq 7.

In this study, the following boundary and initial conditions were used (indices 1 and 2 correspond to ions of the background buffer, while index 3 corresponds to the ionic tracer species)

$$c_1(x = 0, t) = c_1(x = L, t) = c_{1,res}, \, c_2(x = 0, t) = c_2(x = L, t) = c_{2,res}$$

$$c_3(x = 0, t) = 0, \, c_3(x = L, t < t_{start}) = 0, \, c_3(x = L, t_{start} < t < t_{fin}) = c_{3,res}$$

$$c_3(x = L, t > t_{fin}) = 0$$

and

$$\phi(x = 0, t) = V, \, \phi(x = L, t) = 0$$

where $c_{1,res}$ and $c_{2,res}$ are the constant concentrations of the buffer ions in the reservoirs and V is the applied bias. The negatively charged tracer ions are introduced into the channel from the right (cathodic) reservoir in Figures 1 and 2 as a pulse/slug with a constant concentration $c_{3,res} = 5 \, \mu M$. The product of the pulse duration $t_{fin} - t_{start}$ and $c_{3,res}$ defines the total amount of injected tracer molecules, N_{trac}. In this study, $t_{start} = 0$ and $N_{trac} = 6.022 \times 10^7$, while t_{fin} is determined by the magnitude of the applied voltage. The constant N_{trac} facilitates the comparison of simulated enrichment factors for different voltages. The enrichment factor for the tracer zone is determined as the ratio $c_{3,EZ}/c_{3,res}$ where $c_{3,EZ}$ is the highest concentration in the steady-state tracer profile (enrichment zone) in the cathodic compartment of the microchannel. The other physical parameters used in the simulations are given in Table 1. Coupled eqs 2 and 4 were resolved by a parallel code based on lattice algorithms. For the solution of the Poisson and Nernst–Planck equations, respectively, the numerical approaches proposed by Warren[49] and Capuani et al.[50] were employed.

RESULTS AND DISCUSSION

The microfluidic device shown in Figure 2 can be divided into three parts: (1) the anodic compartment connected to a reservoir containing a positive electrode; (2) a negatively charged hydrogel plug with nanometer-sized pores; and (3) the cathodic compartment connected to the other reservoir containing a grounded electrode. The highly cross-linked hydrogel has a nanoporous structure with an estimated average pore size of only a few

(49) Warren, P. B. *Int. J. Mod. Phys. C* **1997**, *8*, 889–898.
(50) Capuani, F.; Pagonabarraga, I.; Frenkel, D. *J. Chem. Phys.* **2004**, *121*, 973–986.

Table 1. Physical Parameters Employed for the Simulations

parameter	anodic compartment	membrane[a,b]	cathodic compartment
diffusion coefficient of a positive ion of buffer solution, m^2/s	1.5×10^{-9}	0.75×10^{-9}	1.5×10^{-9}
diffusion coefficient of a negative ion of buffer solution, m^2/s	1.5×10^{-9}	0.75×10^{-9}	1.5×10^{-9}
diffusion coefficient of a tracer species, m^2/s	0.45×10^{-9}	0	0.45×10^{-9}
dielectric constant	80	80	80
ionic concentration of background solution in reservoirs, mM	5		5
ionic concentration of tracer molecules in reservoirs, mM	0		0.005
volume fixed-charge density of membrane, mM		0.5	

[a] The diffusion coefficient of ions inside the membrane is reduced due to the tortuosity of pores compared with the open, straight microchannel compartments. A reduction by a factor of 2 is assumed. [b] The zero diffusion coefficient of the tracer molecules inside the membrane simulates their complete electrostatic exclusion from the membrane pores at the macroscopic level.

nanometers (~2.0 nm in this study).[28,51] This nanoporous structure greatly increases the electrical resistance of the microfluidic channel. For example, the electrical resistance of a channel in which acrylic acid (AA) is copolymerized with HEMA (AA-*co*-HEMA hydrogel) over the entire length of the channel is ~14 GΩ/cm, and this value can be compared to an otherwise identical open channel, which has a resistance of ~72 MΩ/cm. The nanoporous hydrogel microplug also reduces the hydraulic permeability of the device to such a level that net hydraulic flow (due to pressure gradients which may develop locally in the coupled transport scheme) can be safely neglected compared to the EOF velocity.

In an open O_2 plasma-treated PDMS/glass hybrid microchannel (that is, without the hydrogel microplug) deprotonated surface hydroxyl groups give rise to EOF. The magnitude of this cathodic EOF in terms of the electroosmotic mobility ($\mu_{eo} \approx 4.5 \times 10^{-4}$ cm^2/V s at pH 8.1)[52] exceeds the electrophoretic mobility (μ_{ep}) of negatively charged analytes like fluorescein ($\mu_{ep} \approx -3.0 \times 10^{-4}$ cm^2/V s),[53] and hence no electrophoretic transport toward the anode is possible from the cathodic reservoir. However, in the presence of a hydrogel microplug, the EOF in the system is reduced due to the high electrical and hydraulic resistance of the plug and electrophoretic transport dominates. Consequently, fluorescein can be transported from the cathodic reservoir toward the cathodic hydrogel plug−microchannel solution interface for concentration enrichment.

The fluorescence micrographs in Figure 3a,b demonstrate transient effects on the enrichment of fluorescein in the cathodic microchannel compartment of the device in Figure 2a employing a negatively charged AA-*co*-HEMA hydrogel plug. Under the influence of a 100 V bias, fluorescein in ResB is electrophoretically transported toward the plug. Although fluorescein is smaller (MW ~0.376 kDa, <1.0 nm in diameter) than the estimated pore size (~2.0 nm) of the hydrogel,[28,51] the fixed negative charges on the

(51) Canal, T.; Peppas, N. A. *J. Biomed. Mater. Res.* **1989**, *23*, 1183−1193.
(52) The electroosmotic mobility was determined by measuring the effective mobility of fluorescein in an open O_2 plasma-treated PDMS/glass hybrid microchannel and then comparing it with the electrophoretic mobility of fluorescein.
(53) Gong, M.; Wehmeyer, K. R.; Limbach, P. A.; Heineman, W. R. *J. Chromatogr., A* **2006**, *1125*, 263−269.
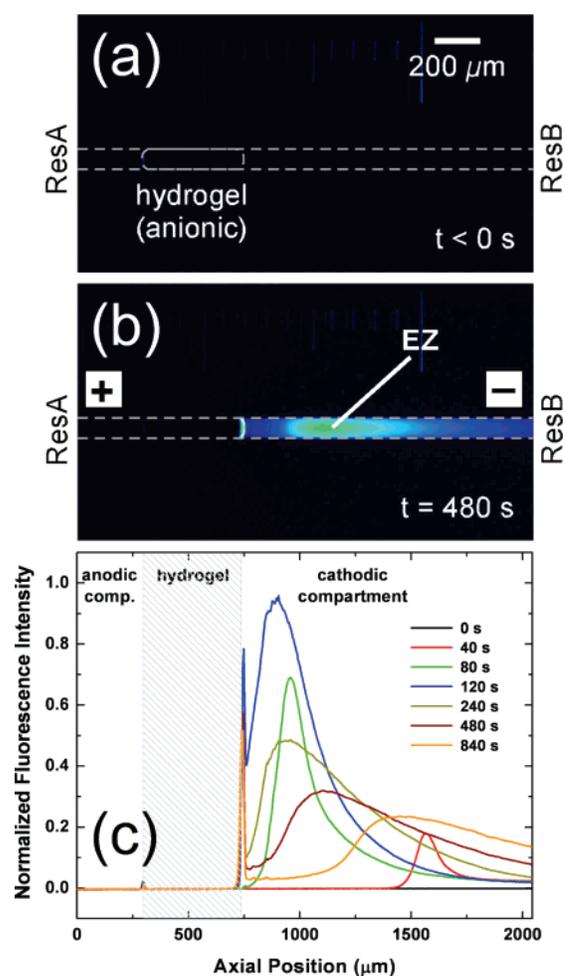
Figure 3. Fluorescence micrographs for fluorescein obtained in the microfluidic device (layout shown in Figure 2a) with an anionic hydrogel microplug (a) before and (b) after applying a forward bias of 100 V for 480 s. The image size was 512 pixels × 290 pixels, and the grayscale applied was 1700−8000 counts per pixel. The micrographs were modified by using a false color scheme (fluorescence intensity decreasing in the order white-green-blue-black). The complete movie is provided in the Supporting Information. (c) Fluorescence intensity profiles for fluorescein obtained parallel to the channel during the forward bias experiment. All fluorescence intensity values were corrected by subtracting the background count before normalization.

hydrogel backbone give rise to Donnan exclusion.[54−56] Specifically, the hydrogel pore size is on the order of the Debye screening length (~3.0 nm for a 10 mM 1:1 electrolyte solution),[57] and therefore comparatively small, but co-ionic fluorescein is excluded from the hydrogel interior.[28] This results in enrichment of fluorescein in the vicinity of the cathodic hydrogel plug−microchannel solution interface (cf. Figure 1). Interestingly, however, the enrichment zone (EZ) is observed a few hundred micrometers away from the hydrogel (Figure 3b), in the bulk solution of the adjoining cathodic microchannel compartment. Figure 3c shows fluorescence intensity profiles for fluorescein obtained along the channel at different times following application of the forward bias. The movie from which these profiles and the micrographs shown in Figure 3a,b were extracted is provided in the Supporting Information (movie S1).

It is important to discuss the location of the EZ as a function of time. In the beginning, when a forward bias is applied across the system, fluorescein molecules from ResB approach the hydrogel ($t < 120$ s). Because the hydrogel is impermeable to fluorescein, it acts as a rigid wall to the leading edge of the approaching EZ, resulting in a sudden rise in the fluorescence intensity at the hydrogel−solution interface. Subsequently, the EZ is displaced from the hydrogel with time. Similar behavior was observed in experiments with ssDNA, and fluorescence intensity profiles for a 22-mer oligonucleotide obtained along the channel are shown in Figure S1 in the Supporting Information.

Figure 4 illustrates selected features of the transient behavior in more detail. Figure 4a is a plot of the electrical current flowing through the device. Zero time corresponds to the application of the electrical field. After an initial rise, the current was observed to decrease rapidly and then approach a near-steady-state value. Enrichment factors as a function of time for fluorescein during application of a 100 V forward bias are shown in Figure 4b. During the first 120 s after application of the bias, the enrichment factor obtains a value of about 100, but it decreases for $t > 120$ s and reaches a near-steady-state value of ~25 after 600 s. Figure 4c shows the location of the fluorescein EZ (cf. Figure 3b) relative to the fixed position of the cathodic hydrogel plug−microchannel solution interface. During the first 120 s of the experiment, the EZ rapidly approaches the hydrogel but is displaced from it after ~240 s. For fluorescein, the EZ was observed to assume a stable position after ~800 s.

On the basis of the behavior of fluorescein in the presence of the anionic hydrogel (Figures 3 and 4), analyte transport can be roughly divided into two stages: an initial transient stage and the approach to steady state. The transient stage is governed by the redistribution of the background electrolyte ions after application of the electrical field during the onset of CP. At electrochemical equilibrium, the cation concentration is higher in the (cation-selective) hydrogel than in the bulk microchannel solutions, whereas anions are excluded from the hydrogel (co-ion exclusion). Accordingly, an electrical phase boundary potential (Donnan potential) between the hydrogel matrix and the bulk liquid phase is established, and it balances the tendency of ions to equalize
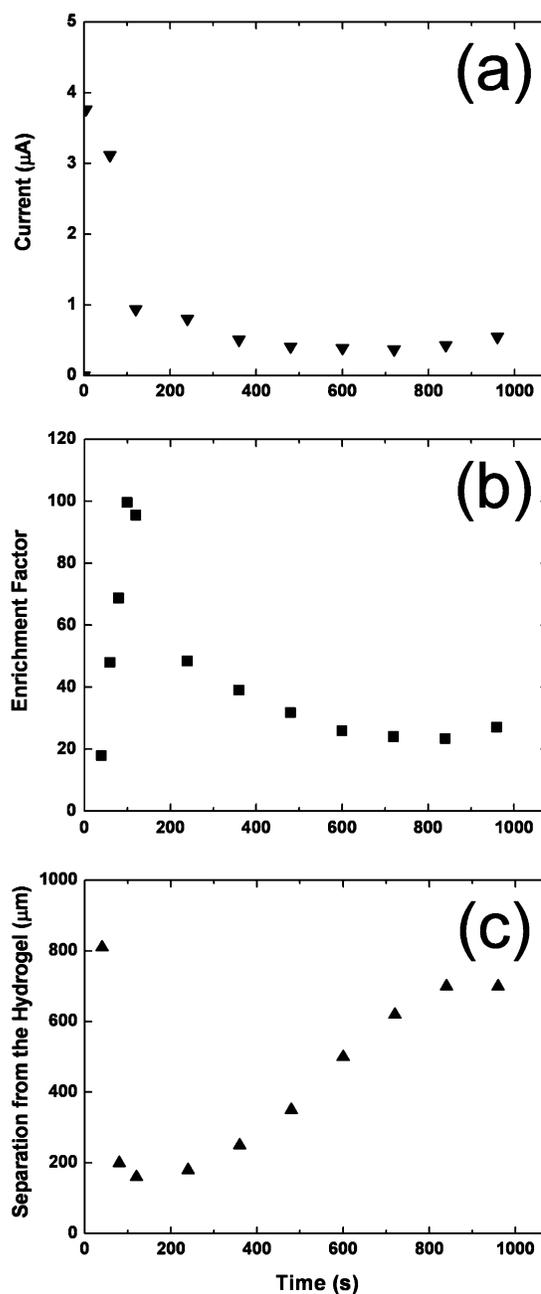
(54) Donnan, F. G. *J. Membr. Sci.* **1995**, *100*, 45−55.
(55) Peppas, N. A.; Khare, A. R. *Adv. Drug Delivery Rev.* **1993**, *11*, 1−35.
(56) Hoffman, A. S. *Adv. Drug Delivery Rev.* **2002**, *43*, 3−12.
(57) Bard, A. J.; Faulkner, L. R. *Electrochemical Methods: Fundamentals and Applications*; John Wiley & Sons, Inc.: New York, 2000.
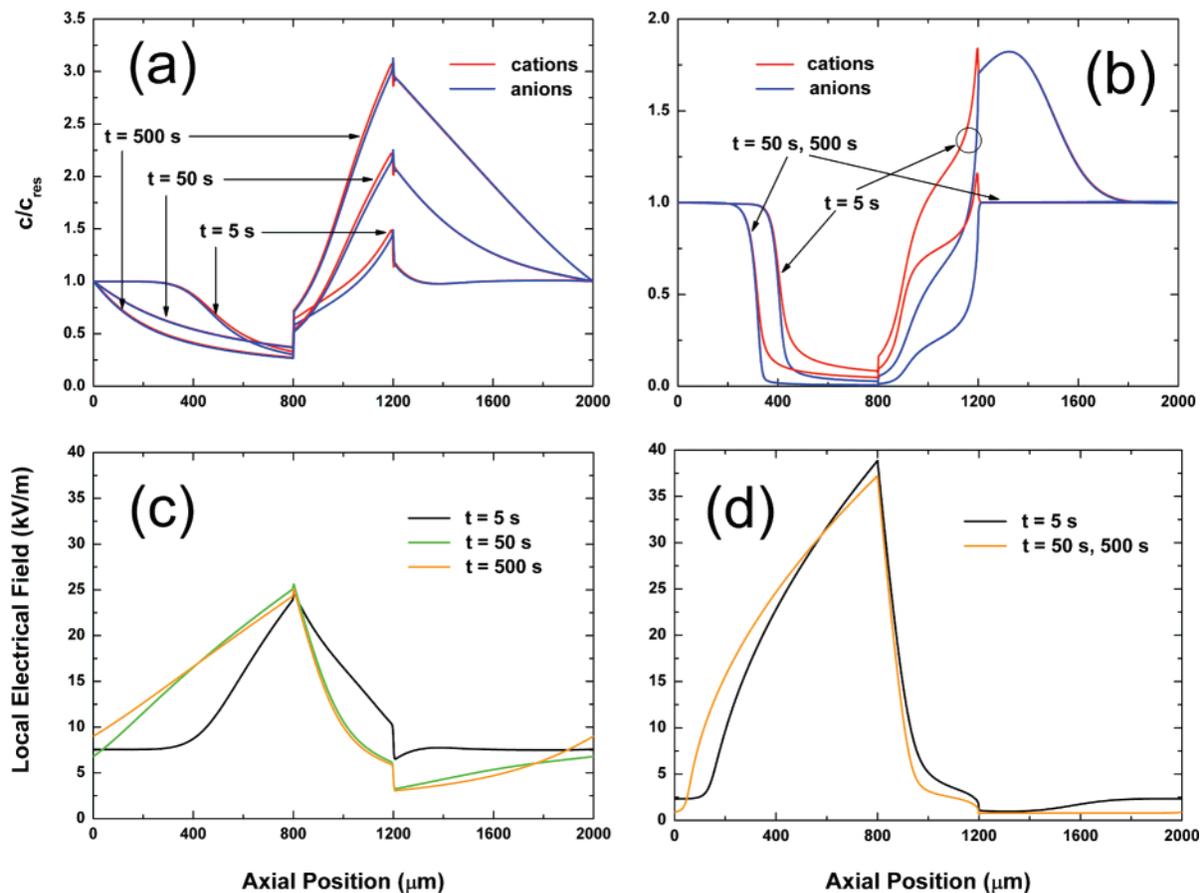
Figure 4. (a) Electrical current through the microfluidic device, (b) enrichment factors, and (c) displacement of the analyte enrichment zone as a function of time in the cathodic microchannel compartment. Applied potential bias, 100 V (forward). The enrichment factors correspond to the respective peak heights in the fluorescence intensity profiles shown in Figure 3c.

the existing concentration differences. As an electrical field is applied to the cation-selective hydrogel plug the transport of electrical current is accomplished nearly exclusively by the counterions (here, cations): the transport number of the counterion (or the sum of the transport numbers of all counterionic species) is nearly unity, i.e., the fractional electrical current carried by the counterions within the hydrogel plug is much larger than the corresponding value within the bulk liquid phases. As a consequence, ionic concentration gradients result at the two hydrogel plug−microchannel solution interfaces. On the anodic side, where counterions (cations) enter the hydrogel in the

Figure 5. Transient concentration distributions for the monovalent cations and anions of the background electrolyte after application of $E_{ext} = 11.1$ kV/m, (a) without EOF inside the membrane and microfluidic channels, (b) with EOF in the device. Corresponding transient distribution of the local electrical field strength, (c) without EOF and (d) with EOF. The correction factor for EOF is assumed to be 0.1. This factor accounts for a reduction of the EOF velocity due to a membrane as compared with the velocity defined by the Helmholtz−Smoluchowski equation for the open microfluidic channel. The volume density of the fixed charge inside the membrane (c_{fix}) is 0.5 c_{res}.

direction of the applied field, the local interplay of convection by EOF, diffusion, and electromigration forms a convective diffusion boundary layer with reduced ion concentrations relative to the bulk solution. It comprises a depleted CP zone. On the opposite side (in the cathodic microchannel compartment) where counterions leave the hydrogel, the electrolyte concentration increases leading to an enriched CP zone. Thus, the formation of CP leads to a dynamic change in the local conductivity which, in turn, results in a redistribution of the electrical potential drop within the system until CP is fully established. Together with the EOF, this modulation of the local electrical field generally affects the tracer EZ as it approaches the cathodic hydrogel plug−microchannel solution interface. In particular, the development of CP, as well as the interplay with the local EOF, explains the transient behavior of the electrical current and the intensity (and location) of the EZ documented experimentally in Figure 4.

Figures 5 and 6, which present the results of our computer simulations, make it possible to analyze in more detail the interplay between the transient distributions of electrolyte ions and local electrical field, as well as the effect of the EOF on these distributions and the concentration enrichment efficiency for a negatively charged analyte. The formation of the depleted CP zone, the region of lowest electrolyte concentration and highest electrical resistance, results in a strong local potential drop (electrical field) in the anodic microchannel compartment, while the opposite

is observed with the enriched CP zone in the cathodic compartment. Steady-state distributions without EOF in the system (Figure 5a,c) were obtained about 500 s after application of a bias. The presence of EOF accelerates the formation of the CP zones and steady-state was established after just 50 s (Figure 5b,d). In Figure 5 the membrane domain covers the distance from $x = 800$ μm to $x = 1200$ μm (cf. Figure 2b).

The duration of the transient period in the systems with and without EOF can be determined by analysis of the temporal behavior of electrical current and local electrical field at the cathodic hydrogel plug−microchannel solution interface (Figure 6a,b). In addition to a faster redistribution of the ion concentrations, a more intense depletion zone is formed in the anodic compartment when EOF is present in the system (Figure 5b vs Figure 5a). This originates in the increased transport of counterions through the membrane by the EOF. As a consequence, an even stronger potential drop occurs in this depleted CP zone (Figure 5d vs Figure 5c), while the cathodic compartment is characterized by a very weak local electrical field (cf. Figure 6b). The most important consequence of this fact is that the anodic electrophoretic migration (depending on the local field strength in the cathodic microchannel compartment) may no longer dominate the cathodic electroosmotic convection.

Figure 7 illustrates this critical interplay of counterdirectional components in species transport for the concentration enrichment
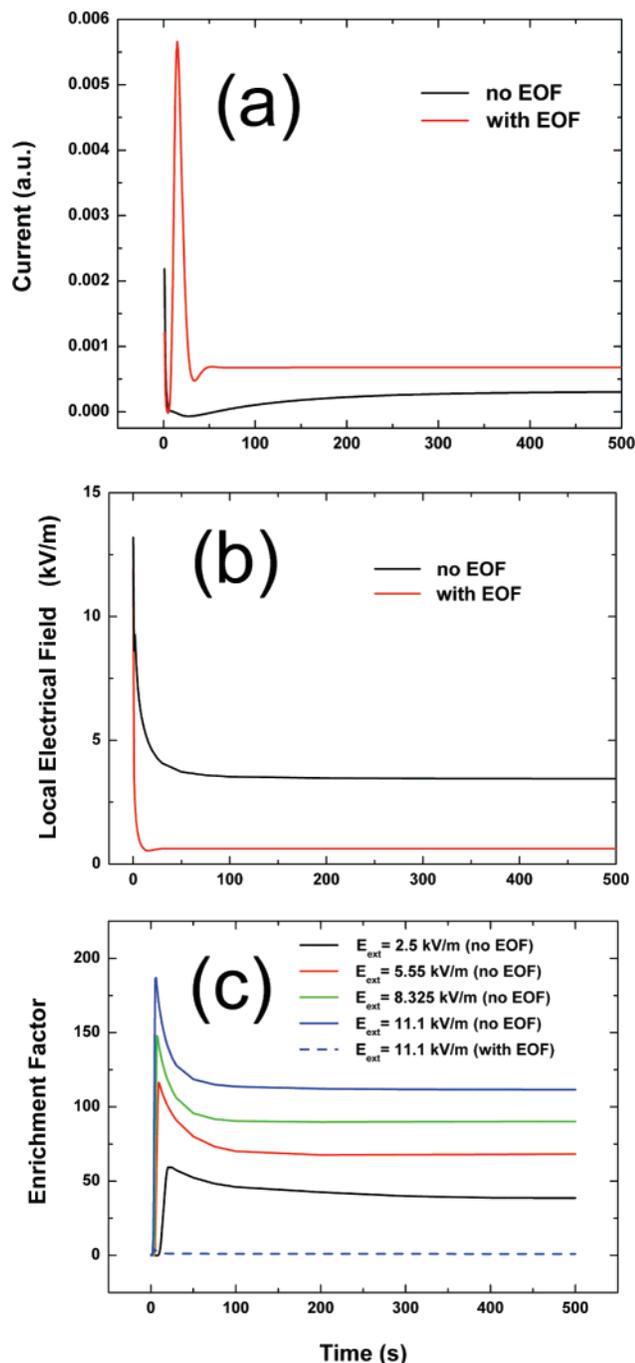
Figure 6. (a) Current flowing through the device after application of $E_{ext} = 11.1$ kV/m without and with EOF, (b) corresponding transient behavior of local electrical field at the cathodic membrane−solution interface, and (c) transient enrichment factor as a function of the applied electrical field strength. The EOF correction factor is assumed to be 0.1.

Figure 7. Transient tracer profiles in the cathodic microchannel compartment which covers the distance from $x = 1200$ μm to $x = 2000$ μm (cf. Figure 2b) for $E_{ext} = 11.1$ kV/m, (a) without and (b) with EOF in the device. The EOF correction factor is assumed to be 0.1.

of a negatively charged analyte. If EOF in the system is suppressed (Figures 6c and 7a), the analyte arrives at the cathodic hydrogel plug−microchannel solution interface within just a few seconds after injection. Further gradual decrease of the local electrical field strength to its asymptotic value (cf. Figure 6b) results in a wider analyte zone (broadened by diffusion) and a reduction of the enrichment factor (Figure 6c, solid lines), while the location of the peak does not change. This picture is very different when EOF is present in the system (Figure 7b). In the beginning, when
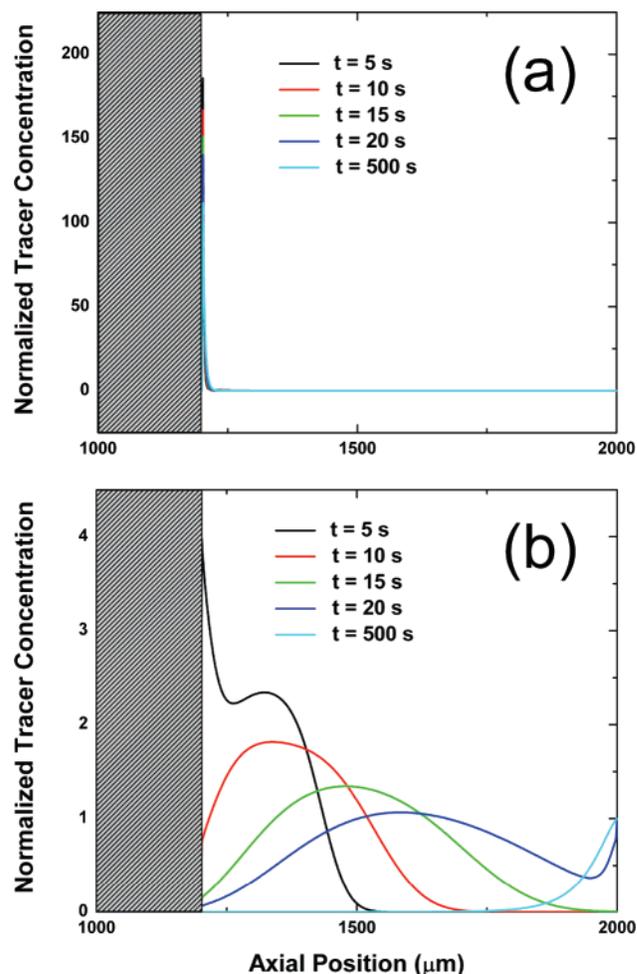
the anodic electrophoretic motion still dominates the cathodic electroosmotic convection, the tracer slug can approach the hydrogel. However, after just 5 s, the gradually decreasing electrophoretic motion (caused by the strong decrease of the local field strength, cf. Figure 6b, which itself originates in the formation of the enriched CP zone) becomes unable to dominate electroosmotic convection and the tracer zone moves away from the hydrogel (see also Figure 6c, dashed line). It is important to note the different scales on the ordinates in Figure 7. This demonstrates the sensitive interplay between hydrogel plug-based EOF and the development of CP (which affects the locally effective field strength) in determining the achievable concentration enrichment efficiency.

The electrokinetic and hydrodynamic effects analyzed in Figures 3−7 become important for a number of similarly designed multifunctional integrated microfluidic devices where discrete nanochannel geometries or nanoporous membranes are currently receiving much attention as modules for on-chip sample precon-centration. The development of CP is almost always an intimate companion, e.g., during the preconcentration of co-ionic analytes at the cathodic interface of a cation-selective membrane as in this work.[28,30,34] As we have demonstrated, an additional problem with the membrane-based approach to concentration enrichment is

caused by EOF inside a charged membrane. Even in narrow channels or pores, a significant volumetric EOF exists which can distort the enriched sample zone on the receiving side, i.e., where the EOF leaves the membrane. Reported nonlinear concentration enrichment factors and the absence of stability in the membrane-based approach to concentration enrichment are explained by the analysis presented in this work. Over time, CP and the associated changes in electrical resistance extend farther leading to nonlinear, often irreproducible, concentration enrichment factors and migration times during subsequent separations.[30,34]

Sample destacking due to transmembrane EOF and CP can be minimized by using a nearly uncharged nanoporous membrane.[25,28] Such neutral membranes enable concentration enrichment by analyte size exclusion, without supporting a significant ion-permselectivity (the prerequisite for CP) or EOF in the nanometer-sized pores. Our current work focuses on characterizing the differences between charged and uncharged membranes for reliable, efficient electrokinetic filtering in microfluidic devices more quantitatively.

CONCLUSIONS

We have analyzed transient electrokinetic effects associated with a negatively charged hydrogel plug immobilized as a transport modulator in a microfluidic channel. The application of an electrical field across the anionic hydrogel triggers CP effects due to the ion-permselectivity of the hydrogel network of nanometer-sized pores. Such hydrogel plugs (or nanoporous membranes) can be used for size- and charge-based electrokinetic analyte preconcentration. However, concentration enrichment with a charged hydrogel is affected by a major redistribution of the local electrical field due to the development of extended CP zones and the simultaneous generation of EOF in the device. The proposed model and experiments provide valuable insight into the fundamental properties of ion-permselective hydrogel plugs or membranes in determining the transport of charged analytes and controlling their enrichment in the adjoining microchannel. In the application of hydrogel microplugs as electrochemical concentrators, the location of the enrichment zone depends sensitively on the interplay between electrophoretic migration of an analyte and the effective electroosmotic convection of the bulk liquid. This peculiar behavior also allows one to envision the possibility of achieving simultaneous concentration enrichment and separation of analytes inside the adjoining microchannel.

SUPPORTING INFORMATION AVAILABLE

Fluorescence intensity profiles for 22-mer ssDNA obtained parallel to the channel incorporating an anionic hydrogel microplug and a movie (MPG format) showing the entire concentration enrichment experiment represented by Figure 3 in the paper. This material is available free of charge via the Internet at http://pubs.acs.org.